PHYSICAL REVIEW C VOLUME 25, NUMBER 1 JANUARY 1982

Production of Kr and Xe isotopes by interaction of ^{232}Th with 0.15–24 GeV protons

H. Sauvageon, S. Regnier, and G. N. Simonoff
Centre d'Etudes Nucléaires de Bordeaux-Gradignan, Laboratoire de Chimie Nucléaire, ERA No 144, Le Haut Vigneau - 33170 - Gradignan, France
(Received 17 June 1981)

Cross sections and thick-target recoil properties of several Kr and Xe isotopes formed in the interaction of ^{232}Th with 0.15–24 GeV protons have been determined in order to study their variations with mass product and incident energy. High sensitivity mass spectrometry has been used to measure noble gas isotopic composition and concentration. The recoil technique, combined with a mathematical formalism based on the two-step model, permits the determination of some characteristics of the nuclear reactions; i.e., the range R, the mean kinetic energy $\langle T \rangle$, the observed products and the excitation energy E^*, and the residual nucleus after intranuclear cascade. The results are discussed in terms of fission and deep spallation mechanism. Fission contributes noticeably to the formation of neutron-excess products at all incident energies, while deep spallation concerns the most neutron-deficient isotopes at energies beyond 1 GeV. This last mechanism is described in terms of coherent interaction between incident protons and target nucleus.

[NUCLEAR REACTIONS Measured σ, $2W(F+B)$ and F/B of various Kr and Xe nuclides formed in interaction of ^{232}Th with 0.15–24 GeV protons.]

I. INTRODUCTION

The production of neutron deficient isotopes with $A \sim 80-140$ formed in the interaction of high energy protons with ^{238}U has been extensively investigated.[1–12] One of the most important results of these experiments is the discovery of a striking change in recoil properties of these nuclides between 1 and 5 GeV. Over this energy interval, the mean range and kinetic energy decrease by a factor of about 2. In addition, the forward to backward ratio (F/B) of these neutron deficient nuclides goes through a maximum in the neighborhood of 3 GeV, after which it decreases with increasing energy. In contrast, neutron-excess isotopes have slightly and monotically decreasing F/B and range variations with increasing incident energy, which are characteristic of fission over a large energy span (0.6–28 GeV).

Moreover, the angular distributions of neutron-deficient products formed in ^{238}U (Refs. 13 and 14) change from forward peaked to sideward peaked between 3 and 11.5 GeV, while the momentum transfer derived from the forward-backward asymmetry approaches zero at the highest energies.

For about 15 years, deep spallation has been essentially interpreted in the framework of a classical, two-step model, in terms of fission, spallation, and fragmentation, or a combination of these processes. But, in that context, it was very difficult to explain the continuous decrease of F/B beyond 3 GeV, the fall of the ranges beyond 1 GeV, and the striking change of angular distributions.

With the growing body of experimental results and the appearance of new concepts in heavy ion reactions and high-energy physics, other models have been proposed for deep spallation. Although these models vary, they are all based on a collective interaction between incident proton and target nucleus.

Even if these new representations of deep spallation do not explain everything, they have aroused still further interest in the interactions of complex nuclei with high-energy protons. Except for very rare experiments,[9] the greatest part of these interactions have been studied by means of radioactive isotopes. Consequently, it would seem to be interesting to consider stable nuclides covering a broad mass range, for a given Z, in order to obtain information concerning both neutron-excess and

deficient isotopes. With this aim, we have determined the cross sections and recoil properties of various krypton and xenon nuclides formed in thorium, using protons of 0.15, 1, 2.5, and 24 GeV.

II. EXPERIMENTAL PROCEDURE

The thick-target—thick-catchers technique is well known and has been described in previous reports from this laboratory.[12,15] The target stacks consisted of 50 μm thorium foil, sandwiched between two pairs of 50 μm aluminum foil. The first pair served as recoil catchers and the second pair as guard foils. Several aluminum foils were added at different locations in the stacks to serve as beam monitors.

The irradiations were carried out in the following accelerators: Orsay (0.15 GeV), CERN (24 GeV), and Saturne I and II (1.05 and 2.5 GeV). At 0.15 and 1.05 GeV, the internal beam was used. The external beam was used at 2.5 and 24 GeV.

The total proton flux through a target was calculated by means of the monitor reaction ^{27}Al $(p,3p\,3n)^{22}$Na, for which the cross sections[16] are 17.2, 15.3, 11.7, and 10 mb, respectively, at 0.15, 1.05, 2.5, and 2.4 GeV. The integrated flux employed varied from 0.3 to 3 $\times 10^{17}$ protons. It was ascertained from the monitor measurements that the targets were properly aligned and that the flux was homogeneous within the stack to better than 5% (1—5%). An interval of several months, at least, separated the irradiations from the analysis.

The techniques employed for the measurement of krypton and xenon produced by nuclear reactions have been described elsewhere.[17,18] Krypton and xenon were extracted by melting the target (or catcher) under a vacuum in a molybdenum crucible, heated by electronic bombardment (600—1800 °C, depending on the metal). The extracted gases were purified by means of two titanium getters and one copper oxyde-palladium getter. Krypton and xenon were analyzed in a 60° sector, 12 cm radius mass spectrometer (a modified MICROMASS 12) with which accurate isotope ratios could be obtained with 10^7 (and sometimes less than 10^7) to 10^{11} atoms of each species, thanks to the small internal volume of the instrument and its excellent behavior under static vacuum conditions.

The mass spectrometer was calibrated by introducing precisely measured quantities of air, prepared in an independent system composed of several known volumes and a capacitance manometer. The isotope ratios were subjected to several corrections, occasioned by memory or pumping effects or isotopic discrimination in the mass spectrometer. Hydrocarbon ions were always negligible, except at masses 78 and 81.

III. RECOIL PROPERTIES DETERMINATION

The following mathematical formalism for the analysis of thick-target—thick-catchers experiments yields the range R of the reaction products and the excitation energy E^* of the cascade residual nucleus.

A. Mathematical treatment

The analysis of the data is carried out using the two-step vector model of high-energy reactions, as first developed by Sugarman *et al.*[19—21] In the first phase of the interaction, the incident particle collides with the nucleus of the target nucleus, causing the emission of cascade particles. An intermediate excited nucleus remains which has a velocity $\vec{v}$.

In the second phase, the intermediate excited nucleus emits particles or fission fragments until krypton or xenon isotopes are finally formed. As a result of this second phase, the recoiling final ion has acquired an additional velocity $\vec{V}$. The angular distribution of $\vec{V}$ in the moving system is assumed to be symmetrical about 90° to the beam direction. The two vectors $\vec{v}$ and $\vec{V}$ are assumed to be uncorrelated.

The final velocity vector of a reaction product is the resultant vector $\vec{v}+\vec{V}$. The relation between the range and the recoil velocity can be conveniently expressed in the laboratory system: $R_{\text{lab}}=K\,|\,\vec{v}+\vec{V}\,|^{N}$. N is a constant characteristic of the nuclear reaction; $N\simeq 1$ for fission and $N\simeq 2$ for spallation.

The mathematical development of the thick-target—thick-catcher recoil experiment theory will express the forward and backward activities, F and B, as developed in Refs. 12 and 15:

$$F=\frac{R}{16\eta^4 W(1+\frac{1}{3}b/a)}$$
$$\times\left\{(1+\eta)^{N+1}\left[\frac{4\eta^2}{N+3}(1+\eta)^2+\frac{4\eta^2}{N+1}(\eta^2-1)\right.\right.$$
$$\left.+\frac{b}{a}\left[\frac{1}{N+7}(1+\eta)^6-\frac{(\eta^2+3)}{N+5}(1+\eta)-\frac{(\eta^4-2\eta^2-3)}{N+3}(1+\eta)^2+\frac{(1+\eta^2)^2(\eta^2-1)}{N+1}\right]\right]$$
$$-(1-\eta^2)^{(N+1)/2}\left[\frac{4\eta^2}{N+3}(1-\eta^2)+\frac{4\eta^2}{N+1}(\eta^2-1)\right.$$
$$+\frac{b}{a}\left[\frac{1}{N+7}(1-\eta^2)^3-\frac{(\eta^2+3)(1-\eta^2)^2}{N+5}\right.$$
$$\left.\left.\left.-\frac{(\eta^4-2\eta^2-3)}{N+3}(1-\eta^2)+\frac{(1+\eta^2)^2(\eta^2-1)}{N+1}\right]\right]\right\}. \quad (1)$$

If η is replaced by $-\eta$, relation (1) gives the expression for B [denoted (1a)].

In these equations, R is the mean range in the target material corresponding to the velocity V, η is the ratio of the cascade velocity to the second step velocity V (the perpendicular component of the cascade velocity, $v_\perp$, is assumed to be zero), b/a is the anisotropy parameter, and W is the target thickness.

B. Range and kinetic energy

Assuming $b/a=0$ relations (1) and (1a) give

$$2W(F+B)=F(R,\eta,N)\,,$$
$$W(F-B)=G(R,\eta,N)\,,$$

and the ratio Q_{cal} is only a function of η and N:

$$Q_{\text{cal}}=2W(F+B)/(F-B)\,.$$

In a computer calculation, N was varied from 1 to 2 in steps of 0.1 and η from 0 to 1 in steps of 0.01. The η and N values are considered acceptable if $(Q_{\text{cal}}-Q_{\text{exp}})/Q_{\text{exp}}<1\%$; Eqs. (1) and (1a) then lead to two different values of R. Acceptable combinations of R and N must, moreover, satisfy the range-energy relation $R=KV^N$ (in the c.m. system). The range finally adopted is the one that corresponds to the value of N obtained from the Northcliffe-Schilling tables.[22]

The mean kinetic energy $\langle T\rangle$ has been calculated with the Northcliffe-Schilling range-energy relations. The range had to be corrected for scattering.

C. Average excitation energy of residual cascade nucleus

The velocity v imparted to the target nucleus by cascade can be determined from $T=\frac{1}{2}AV^2$ and η. Intranuclear cascade calculations have shown a correlation between momentum component P_t, transferred to the target nucleus and parallel to the beam and the average excitation energy E^*, of cascade residues. Using Metropolis calculations,[23] Porile[24] found that the relation

$$\frac{E^*}{E_{\text{CN}}}=0.8\frac{P_t}{P_{\text{CN}}} \quad (2)$$

was satisfied for many targets and bombarding energies up to 1.8 GeV. In Eq. (2), P_{CN} and E_{CN} are, respectively, the momentum and excitation energy of a hypothetical compound nucleus formed by the fusion of proton and target nucleus. Kaufman *et al.*[25] have tested this correlation at 3 GeV and have found it valid for this case also.

IV. RESULTS

A. Cross sections

Table I gives the cross sections for various krypton and xenon isotopes formed in thorium at 0.15, 1, 2.5, and 24 GeV. The last column gives the ratio $\sigma_{2.5}/\sigma_{0.15}$ of cross sections at 2.5 and 0.15 GeV. This ratio is of interest when comparing neutron-excess and neutron-deficient nuclides. All the cross sections are cumulative. In general, each value is the average of three independent measurements. The uncertainties have been determined as explained elsewhere[26]: The total uncertainty of a cross section measurement is generally from 10–20%. The mean of the independent measurements x_i is then calculated, weighting each of these by the inverse of the square of its uncertainty, Δx_i. Thus σ is given by

$$\sum_i (x/\Delta x^2)/\sum_i (1/\Delta x)^2 .$$

The uncertainty given in Table I is the standard deviation from the mean of the independent measurements, or the quantity

$$\Delta\sigma+[\sum(1/\Delta x)^4]^{1/2} ,$$

whichever is the larger.

B. Recoil properties

Table II gives the experimental values of the forward-to-backward ratio F/B. This ratio represents a measure of the forward momentum transferred to the target nucleus in the reaction which leads to the isotope considered.

Table III gives the values of the experimental ranges in the target material, $2W(F+B)$ in mg/cm^2. The ranges have been corrected for scattering at the target-catcher interface and for edge effects.

Table IV gives mean kinetic energy $\langle T \rangle$ (in MeV) calculated by the method described in Sec. II B above. In Table V, experimental values of this parameter are compared with those calculated theoretically, $\bar{E}$, by Nix and Swiatecki,[27] according to the liquid drop model. The ratio $\langle T \rangle/\bar{E}$ is a good test for fission.

Table VI gives the values (in MeV) of the excitation energies of the residual cascade nuclei leading to the various isotopes considered in this work. The errors given in Tables II to IV are the root mean square deviations observed for repeated experiments.

TABLE I. Cumulative krypton and xenon nuclides cross sections, in mb, measured in thorium bombarded with 0.15, 1, 2.5, and 24 GeV protons. The last column gives the cross sections ratio, $\sigma_{2.5}/\sigma_{0.15}$, at 2.5 and 0.15 GeV.

Isotope	Proton energy (GeV) 0.15	1	2.5	24	2.5/0.15
Kr 78		0.35±0.06	1.1±0.2	2.1±0.3	
80	0.23 ±0.02	8.0 ±0.7	9.7±1.7	10.7±1.4	17±3
81	0.050±0.006	4.44±0.76	7.1±1.3	9.3±1.2	45±9
82	2.17 ±0.23	16.5 ±1.4	15.2±3.0	15.6±2.6	7.0 ±2.1
83	14.4 ±1.5	28.0 ±3.5	21.8±3.4	20.6±3.6	1.5 ±0.4
84	17.0 ±1.8	28.7 ±4.1	20.4±3.1	18.7±3.4	1.2 ±0.3
85	5.76 ±0.62	10.1±1.5	6.2±1.0	5.5±1.0	1.1 ±0.3
86	17.9 ±1.9	21.2 ±4.0	8.8±1.3	10.7±2.0	0.49±0.12
Xe 124	0.020±0.006	2.06±0.33	6.3±1.1	7.2±1.1	315±142
126	1.42 ±0.23	7.1 ±0.8	9.5±1.8	11.3±1.7	6.8 ±2.3
128	7.5 ±1.2	12.1 ±1.5	12.2±2.2	13.2±2.0	1.6 ±0.5
129	3.2 ±0.5	8.4 ±0.9	10.3±1.8	11.7±1.7	3.2 ±1.1
130	13.1 ±2.1	11.6 ±2.5	5.6±1.0	6.2±1.1	0.43±0.14
131	21.9 ±3.5	18.9 ±4.0	15.2±2.9	17.9±2.6	0.69±0.23
132	21.0 ±3.3	14.1±3.8	7.3±1.4	9.1±1.7	0.43±0.14
134	14.7 ±2.3	9.0±2.5	5.4±1.0	6.7±1.2	0.37±0.12
136	9.1 ±1.4	6.3±1.6	3.9±0.8	5.9±1.1	0.43±0.15

TABLE II. Experimental values of the forward to backward ratio F/B for krypton and xenon isotopes formed in thorium bombarded with 0.15, 1, 2.5, and 24 GeV protons.

Isotope	Proton energy (GeV) 0.15	1	2.5	24
Kr 78		1.33±0.07	1.63±0.15	1.16±0.07
80	1.13±0.08	1.27±0.08	1.35±0.10	1.16±0.10
81		1.36±0.12	1.54±0.11	1.12±0.15
82	1.14±0.10	1.26±0.08	1.31±0.07	1.13±0.09
83	1.09±0.08	1.23±0.04	1.28±0.12	1.10±0.08
84	1.09±0.05	1.21±0.05	1.15±0.08	1.11±0.03
85	1.10±0.07	1.21±0.06	1.16±0.05	1.05±0.07
86	1.10±0.05	1.14±0.09	1.08±0.09	1.07±0.06
Xe 124		1.44±0.06	1.57±0.05	1.33±0.03
126	1.23±0.05	1.35±0.06	1.48±0.06	1.25±0.05
128	1.23±0.04	1.24±0.03	1.40±0.08	1.28±0.09
129	1.22±0.07	1.29±0.07	1.35±0.03	1.16±0.03
130	1.13±0.03	1.15±0.04	1.15±0.07	1.08±0.04
131	1.17±0.05	1.19±0.08	1.31±0.09	1.20±0.07
132	1.14±0.03	1.09±0.07	1.11±0.04	1.10±0.06
134	1.11±0.05	1.09±0.04	1.06±0.07	1.05±0.04
136	1.11±0.07	1.10±0.04	1.13±0.03	1.07±0.04

TABLE III. Experimental recoil ranges in units of mg/cm^2 $[2W(F+B)]$ of krypton and xenon isotopes formed in thorium with 0.15, 1, 2.5, and 24 GeV protons. The data have been corrected for scattering.

Isotope	Proton energy (GeV) 0.15	1	2.5	24
Kr 78		8.47±0.64	5.49±0.56	4.67±.42
80	9.10±0.72	10.39±0.48	8.05±0.63	7.06±0.37
81		10.13±0.79	7.75±0.48	6.63±0.26
82	10.36±0.68	10.01±0.41	8.62±0.41	8.19±0.41
83	11.05±0.46	10.02±0.36	8.82±0.57	8.47±0.32
84	11.14±0.59	10.00±0.43	9.11±0.42	8.88±0.36
85	10.55±0.40	9.82±0.34	9.29±0.37	9.72±0.61
86	10.97±0.52	9.86±0.65	9.99±0.51	9.34±0.34
Xe 124		7.00±0.34	5.16±0.22	3.83±0.17
126	7.69±0.24	7.04±0.39	5.68±0.24	4.53±0.14
128	7.80±0.18	7.46±0.27	6.10±0.23	5.32±0.36
129	7.68±0.31	7.54±0.34	6.23±0.33	5.84±0.19
130	8.08±0.25	7.66±0.27	8.32±0.41	8.10±0.30
131	8.30±0.28	6.77±0.36	6.71±0.46	6.99±0.44
132	8.19±0.33	7.14±0.28	8.17±0.27	8.18±0.35
134	8.11±0.24	8.11±0.29	8.29±0.24	8.08±0.33
136	8.11±0.30	8.10±0.33	7.78±0.29	7.90±0.30

TABLE IV. Mean kinetic energy $\langle T \rangle$ (in MeV), of krypton and xenon isotopes formed in thorium bombarded with 0.15, 1, 2.5, and 24 GeV protons.

Isotope	Proton energy (GeV) 0.15	1	2.5	24
Kr 78		60.2±8.4	25.6±4.3	18.8±2.6
80	63.1±9.6	88.2±7.8	51.2±7.0	39.7±3.4
81		83.8±12.9	48.0±5.9	34.6±2.6
82	81.8±10.6	81.9±6.7	58.5±5.4	51.7±5.2
83	89.3±7.4	78.6±5.7	60.7±7.4	54.3±4.1
84	92.8±9.7	78.8±6.8	63.8±5.5	58.7±4.6
85	82.4±6.3	74.7±5.1	68.0±5.3	68.7±8.8
86	86.9±8.3	72.3±9.4	70.2±7.3	6.37±4.3
Xe 124		47.6±4.4	28.4±2.0	18.4±1.2
126	54.9±3.0	48.0±5.1	32.8±2.3	23.6±1.1
128	55.9±2.2	53.0±3.7	37.1±2.4	29.8±3.3
129	55.1±3.7	51.5±4.4	38.1±3.5	34.2±1.9
130	61.0±3.3	55.6±3.5	64.7±6.2	62.2±4.5
131	60.9±3.6	43.8±4.2	42.7±5.2	46.4±5.4
132	59.5±4.1	48.3±3.5	62.0±4.0	62.0±5.1
134	58.1±3.0	58.6±3.5	63.2±3.6	59.8±4.8
136	57.6±3.6	57.5±4.0	55.2±4.0	55.9±4.1

V. DISCUSSION

Table VII shows the variation of N/Z ratios for $^{78-86}$Kr and $^{124-136}$Xe around the stability line. Effects from N/Z will be emphasized in the following discussion.

A. Cross sections, F/B ratios, and experimental ranges $2W(F+B)$

Differences of production mechanisms between neutron deficient and neutron excess isotopes notably concern cross sections, F/B ratios, and experi-

TABLE V. $\langle T \rangle / \bar{E}$ ratio of experimental to calculated kinetic energy (see text).

Isotope	Proton energy (GeV) 0.15	1	2.5	24
Kr 78		0.62±0.09	0.26±0.04	0.19±0.03
80	0.65±0.10	0.90±0.08	0.62±0.08	0.41±0.04
81		0.86±0.13	0.49±0.06	0.35±0.03
82	0.84±0.11	0.84±0.07	0.60±0.06	0.53±0.05
83	0.91±0.08	0.80±0.06	0.62±0.08	0.56±0.04
84	0.95±0.10	0.81±0.07	0.65±0.06	0.60±0.05
85	0.85±0.06	0.77±0.05	0.70±0.05	0.71±0.09
86	0.90±0.09	0.75±0.10	0.72±0.08	0.66±0.04
Xe 124		0.63±0.06	0.37±0.03	0.24±0.02
126	0.72±0.04	0.63±0.07	0.43±0.03	0.31±0.01
128	0.76±0.03	0.72±0.05	0.51±0.03	0.41±0.05
129	0.75±0.05	0.70±0.06	0.52±0.05	0.47±0.03
130	0.85±0.05	0.78±0.05	0.90±0.09	0.87±0.06
131	0.85±0.05	0.61±0.06	0.60±0.07	0.65±0.08
132	0.85±0.06	0.69±0.05	0.88±0.06	0.88±0.07
134	0.85±0.04	0.85±0.05	0.92±0.05	0.87±0.07
136	0.86±0.05	0.86±0.06	0.83±0.06	0.84±0.06

TABLE VI. Excitation energies E^* (in MeV) of residual cascade nuclei, leading to krypton and xenon isotopes, formed by interaction of thorium with 0.15, 1, 2.5, and 24 GeV protons.

Isotope	Proton energy (GeV) 0.15	1	2.5	24
Kr 78		294± 50	443±92	142±23
80	61±10	303± 48	409±69	204±31
81		385±103	552±78	158±30
82	74±16	284± 36	402±48	180±34
83	51±11	244± 28	356±60	142±26
84	52± 7	229± 28	205±29	183±19
85	54± 8	222± 24	243±30	197±31
86	55± 7	139± 30	109±28	126±19
Xe 124		252± 34	306±33	183±19
126	75± 8	210± 27	283±34	161±18
128	74± 7	173± 19	260±31	211±37
129	73±10	167± 24	236±31	150±15
130	46± 4	80± 9	140±26	101± 9
131	58± 6	117± 17	231±43	195±34
132	47± 4	63± 8	125±11	120±15
134	37± 5	69± 8	125±19	117±13
136	37± 6	71± 8	119±13	94± 9

mental ranges $2W(F+B)$. A good representation of these differences is obtained by showing on the same graph the variation of these three experimental data with incident energy, as Biswas and Porile[11] have done for cerium, lanthanum, and barium isotopes. The results obtained for the eight krypton isotopes and the nine xenon isotopes studied here are presented in Fig. 1 (Kr) and Fig. 2 (Xe).

In the case of the krypton isotopes, the behavior of the three parameters σ, F/B, and $2W(F+B)$ changes progressively from that of neutron-deficient (increasing cross sections, F/B ratios showing a maximum at about 2.5 GeV, and decreasing ranges between 1 and 24 GeV) to that of neutron-excess nuclides.

^{78}Kr, ^{80}Kr, ^{81}Kr, and ^{82}Kr all show the characteristics of neutron-deficient isotopes, but not to the same extent. Specifically, these characteristics are less pronounced for ^{82}Kr (particularly for the fall of the ranges beyond 1 GeV) than for the other three isotopes. ^{83}Kr and ^{84}Kr represent two transition isotopes. Their cross sections seem to go through a maximum at about 1 GeV and the values at 2.5 and 24 GeV are intermediate between those at 0.15 and 1 GeV. The maximum at 2.5 GeV for the F/B ratios is less distinct, as is the fall in the ranges beyond 1 GeV.

^{85}Kr and ^{86}Kr exhibit the classical behavior of neutron-excess isotopes: slight decrease or constan-

TABLE VII. Variation around the stability line of N/Z ratios for $^{78-86}$Kr and $^{124-136}$Xe.

Kr	78	80	81	82	Stability	83	84	85	86	
N/Z	1.17	1.22	1.25	1.28	1.292	1.31	1.33	1.36	1.39	
Xe	124	126	128	129	Stability	130	131	132	134	136
N/Z	1.30	1.33	1.37	1.39	1.393	1.41	1.43	1.44	1.48	1.52

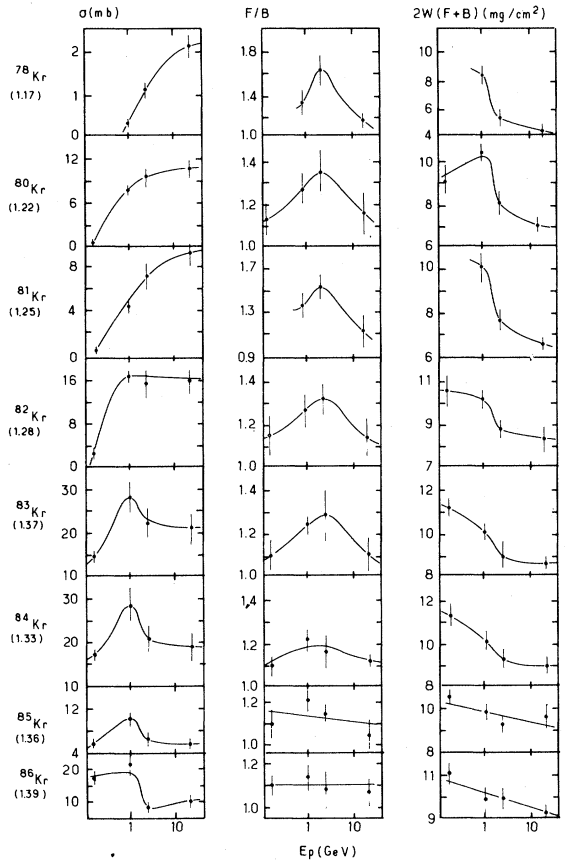

FIG. 1. Incident energy dependence of σ (left), F/B (middle), and range (right) of krypton isotopes formed by interaction for ^{232}Th with high-energy protons. Numbers in brackets are the N/Z ratios of the product nucleus.

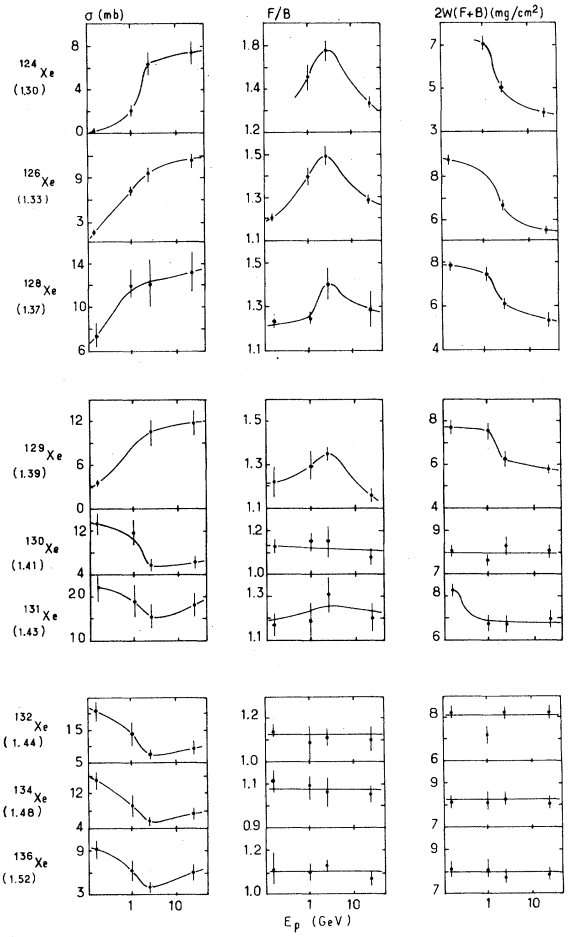

FIG. 2. Incident energy dependence of σ (left), F/B (middle), and range (right) of xenon isotopes formed by interaction for ^{232}Th with high-energy protons. Numbers in brackets are the N/Z ratios of the product nucleus.

cy of F/B ratios and ranges between 0.15 and 24 GeV. With regard to cross sections, another parameter may be used to differentiate neutron-deficient and neutron-excess products, i.e., the ratio $\sigma_{2.5}/\sigma_{0.15}$ of the cross section at 2.5 and 0.15 GeV. For krypton isotopes, this ratio decreases with increasing neutron number, the greatest value being that for ^{81}Kr. It may be noted that the neutron-deficient characteristics of this isotope (increasing cross sections, maximum of F/B, and decrease of ranges) are more pronounced than for ^{80}Kr. This is due to the fact that ^{81}Kr is protected towards β^- isobars, which is not the case of ^{80}Kr.

In the case of xenon isotopes, the situation is clearer still: ^{124}Xe, ^{126}Xe, ^{128}Xe, and ^{129}Xe show the behavior of neutron-deficient nuclides, these characteristics being all the more marked as these isotopes are neutron poor. ^{130}Xe, ^{132}Xe, ^{134}Xe, ^{136}Xe, and, to a lesser extent, ^{131}Xe exhibit the characteristics of neutron-excess nuclides. The ^{131}Xe excitation function is similar to those of other neutron-rich isotopes, but the F/B ratios seem to go through a slight maximum at 2.5 GeV and the range falls by about 15% between 0.15 and 1 GeV.

The ratios $\sigma_{2.5}/\sigma_{0.15}$ (Table I) show that the distinction between neutron-deficient and neutron-excess nuclides is sharper for xenon than for krypton. For xenon, all the values of this ratio are higher than 1.5 for neutron-poor isotopes and smaller than 0.7 for neutron-rich isotopes; the fall of this ratio from ^{129}Xe to ^{130}Xe approaches a factor of about 8.

B. Test for fission: ratios $\langle T \rangle / \bar{E}$

As indicated above, the comparison between experimental kinetic energies $\langle T \rangle$ and those calculated theoretically, $\bar{E}$, by Nix and Swiatecki[27] provides an interesting indication of the fission contribution. However, agreement between experimental and calculated values does not mean that the production mechanism is necessarily binary fission, but simply that the results are consistent with such a process.

As expected, all the values $\langle T \rangle / \bar{E}$ (Table V) are less than unity, since in the calculations, the target nucleus is assumed to be the fissioning nucleus. The mass difference due to nucleons lost during the cascade step and to prefission evaporation is not taken into account.

For krypton as well as for xenon, this ratio is greater than 0.60 for all isotopes at 0.15 and 1 GeV. It seems reasonable to suppose that fission is the main mechanism leading to all these isotopes at energies up to 1 GeV. However, for relatively low energies (0.15 and 1 GeV), we note in many cases that the values of $\langle T \rangle / \bar{E}$ are a little smaller for neutron-deficient than for neutron-excess nuclide. This fact may be explained by assuming that the fissioning nuclei responsible for neutron-poor isotopes are lighter than those leading to neutron-rich products. Such a hypothesis is confirmed by the excitation energies of residual cascade nuclei (Table VI). Tables IV and VI show—essentially for xenon at 1 GeV—that lower kinetic energies (neutron deficient case) correspond to higher excitation energies, and that the reverse is true for neutron-excess isotopes. High excitation energies correspond to lighter cascade and fissioning nuclei than do low excitation energies. Consequently, neutron-deficient fission fragments have less kinetic energy than neutron excess. This appears in Fig. 3.

Differences between neutron-poor and neutron-rich nuclides become important at 2.5 and still more so at 24 GeV. This is apparent in Fig. 4, which represents the variations of $\langle T \rangle / \bar{E}$ with incident energy for six xenon isotopes: ^{130}Xe, ^{134}Xe, and ^{136}Xe have $\langle T \rangle / \bar{E}$ ratios approximately constant, whatever the incident energy. Consequently, for such nuclides, fission may be the principal mechanism responsible for their formation over the whole energy range considered. The behavior of ^{124}Xe, ^{126}Xe, and ^{129}Xe is very different: Their $\langle T \rangle / \bar{E}$ values decrease with increasing incident energy, particularly between 1 and 2.5 GeV. For such nuclides, fission may not be significant beyond 1 GeV. This will be discussed below. For

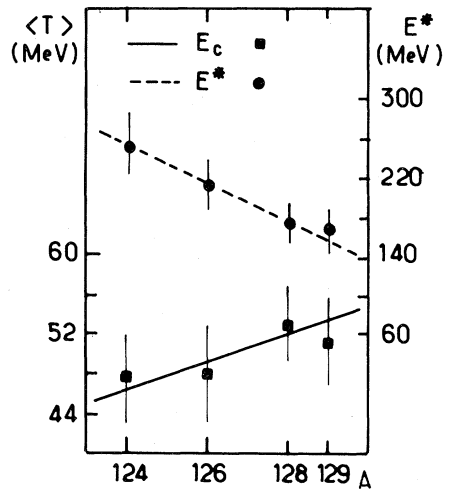

FIG. 3. Variation of mean kinetic energy and excitation energy with isotope mass A for some xenon nuclides.

xenon, in conclusion, all the isotopes seem to be mainly produced by fission at 0.15 and 1 GeV. At 2.5 and 24 GeV, only the most neutron-excess nuclides, ^{130}Xe, ^{132}Xe, ^{134}Xe, ^{136}Xe and, to a lesser extent ^{131}Xe (because of cumulative effects of β^+ isobars), are still formed by the same mechanism.

For krypton as well, fission may be involved for all isotopes at 0.15 and 1 GeV. At 24 GeV, however, the fission contribution increases with mass number, but the distinction between neutron deficient and neutron excess isotopes is less marked than for xenon. This is due to cumulative effects from both the β^+ and β^- sides of the stability line

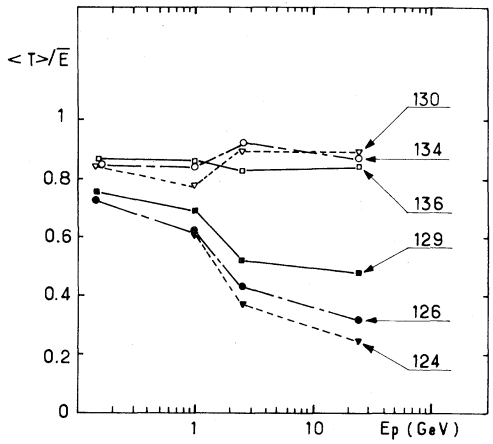

FIG. 4. Incident energy dependence of experimental to calculated kinetic energy $\langle T \rangle / \bar{E}$ ratio for six xenon isotopes (^{124}Xe, ^{126}Xe, ^{129}Xe, ^{130}Xe, ^{134}Xe, and ^{136}Xe).

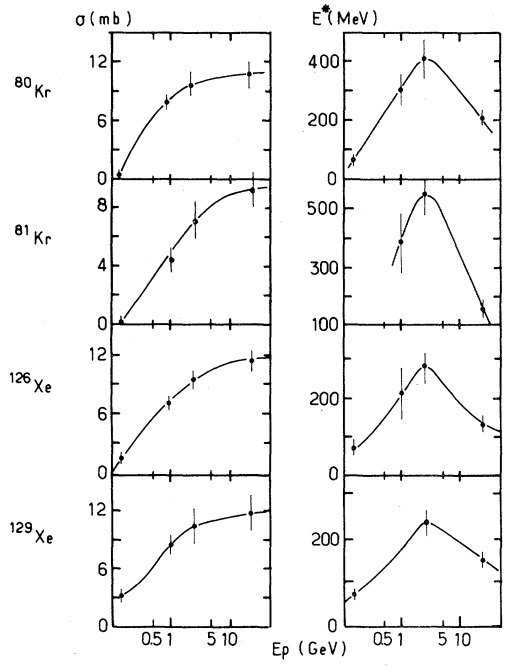

FIG. 5. Incident energy dependence of cross sections and excitation energies for four neutron deficient isotopes.

which contribute to the production of some nuclides (^{82}Kr, ^{83}Kr, and ^{84}Kr).

C. Neutron-deficient isotopes at 2.5 and 24 GeV

It has been seen above that the values of the average excitation energies of the residual cascade nuclei can be obtained from measured recoil data. It is very instructive to compare, for neutron deficient isotopes, the shape of the excitation functions with the variation of the excitation energy E^* versus incident energy. Figure 5 shows results for ^{80}Kr, ^{81}Kr, ^{126}Xe, and ^{129}Xe. Whereas the excitation functions are increasing even at 2.5 and 24 GeV, the average excitation energies go through a maximum at about 2.5 GeV, then decrease strongly. This behavior is not understandable in the framework of the conventional two step model. Porile and Sugarman[28] showed that the shift of the excitation functions toward the formation of high-energy reaction products (here neutron deficient isotopes) could only be explained if, after a strong increase up to a few GeV, the excitation energy should remain essentially constant. Figure 5, however, shows the opposite behavior for E^*. A possible explanation lies in the possibility that the P_t-E^* relation [Eq. (2)] breaks down for neutron-deficient production. This relation is assumed to hold up to 1.8 GeV even up to 3 GeV.[9] Although some authors have maintained that it was incorrect to use it beyond a few GeV, valid results for E^* are obtained from Eq. (2) when $E_p > 3$ GeV for several high-energy nuclear reactions such as neutron-rich production by GeV fission. Consequently, this relation may be used at high energy in some cases. On the other hand, as mentioned above, the P_t-E^* correlation was obtained from classical cascade calculations.[23] Thus, the breakdown of this correlation beyond 2.5 GeV may mean that, at such energies, the classical cascade model ceases to be valid for neutron-deficient nuclides production. This assumption is corroborated by some experimental features pointed out by several workers.[29–31] One of these is the behavior of multiplicity ratio $R_A = \langle n \rangle_A / \langle n \rangle$, where $\langle n \rangle_A$ and $\langle n \rangle$ are, respectively, the average number of charged particles emitted in particle-nucleus collisions and in particle-particle collisions. This ratio R_A is nearly independent of incident energy and increases by a factor of only about 2 from hydrogen to uranium.[30] If secondary particles effectively participated in an intranuclear cascade, R_A would increase more sharply with target mass. Consequently, it has been supposed that the fast secondary particles do not interfere in the cascade step. This assumption is the basis of several collective models, such as the energy flux model,[32] the collective tube model,[31] and the effective target model.[30] All these models share the idea of a collective interaction between the incident particle and the target nucleus. According to these models, a highly relativistic particle may act collectively with the nucleons of the target along its path, in contrast to a conventional intranuclear cascade consisting of a number of collisions with individual quasifree nucleons.

Several authors[11,14,33] have tried to apply these new concepts of high-energy physics to proton-nucleus interactions at a few GeV, particularly in an attempt to understand deep spallation reactions. According to these authors, the collective interaction between incident proton and target nucleus involves the ejection of a "tube" of nuclear matter in the forward direction, leaving behind a highly un-

stable residual nucleus. This residue may break up in two or more fragments, preferentially emitted transversely to the beam direction. Since the ejected tube carries off the greater part of the momentum of the incident proton, relatively little is transferred to the spectator residue. Thus, the observed products resulting from deexcitation of these fragments would have low F/B values and sideways-peaked angular distributions. These features have been observed in various experiments.

Such a collective interaction model qualitatively explains some observed phenomena in deep spallation reactions. But, as mentioned by Pandian and Porile,[14] several major problems remain. Certain experimental results, such as the decrease of the ranges of neutron-deficient products, show that extensive mass loss occurs prior to breakup. This phenomenon is, currently, not well understood without the intervention of an important momentum transfer which is in the opposite to the experimental observations.

In the actual state of our knowledges, it is very difficult to have a clear idea of the nature of deep spallation reactions and, particularly of the production of neutron-deficient isotopes. However, perceptible progress has been realized in recent years. It appears now that the transition between fission and deep spallation for neutron-deficient nuclides may be understood as a change of the first step of the reaction from a classical intranuclear cascade to a collective interaction. The nature of the latter is not yet very clear. Moreover, it seems that the impact parameter of the initial collision plays an important role in the later evolution of the interaction. A collective interaction involves a sufficient amount of nuclear matter along the incident proton direction. Central, or near central, collisions should cause such processes. In contrast, peripheral collisions would still lead to classical intranuclear cascade and, thus, to be responsible of binary fission.

VI. CONCLUSIONS

The thick-target—thick-catcher technique and mass spectrometry measurements have been used to study the production of various krypton and xenon isotopes. The incident energy dependence of cross sections, F/B ratios, and experimental ranges $2W(F+B)$ and the comparison between experimental and calculated kinetic energies are compatible with the following two mechanisms. Fission is responsible for the formation of all the isotopes at 0.15 and 1 GeV, then only for that of the most neutron excess (^{85,86}Kr and $^{130-136}$Xe) at 2.5 and 24 GeV. Deep spallation becomes the principal mechanism for most neutron-deficient nuclides (^{78,80,81}Kr and ^{124,126,128,129}Xe) beyond 1 GeV. For xenon isotopes the deep spallation contribution depends on the N/Z ratio, but the separation is distinct between neutron-excess and neutron-deficient products. Such is not the case for krypton, since $^{82-84}$Kr represents, in some way, a transition group between neutron-rich and neutron-poor nuclides. The transition between fission and deep spallation is interpreted as a change in the nature of the first step of the nuclear reaction from a classical intranuclear cascade to a collective interaction between incident proton and target nucleus.

ACKNOWLEDGMENTS

The cooperation and assistance of the coordination teams of the Orsay, CERN, and Saclay accelerators is gratefully acknowledged. The authors would like to thank N. T. Porile for useful discussions. Collaboration of F. Brout for technical assistance and of A. Mackenzie Peers for the English text are also appreciated. This work was partly supported by the Délégation Générale à la Recherche Scientifique et Technique (Contract No. 74-0931).

[1]J. Alexander, C. Baltzinger, and M. F. Gadzik, Phys. Rev. 129, 1826 (1963).
[2]R. Brandt in *Proceedings of the Symposium on the Physics and Chemistry of Fission, Salzburg, 1965* (I.A.E.A., Vienna, Austria, 1965), Vol. 2, p. 329.
[3]J. A. Panontin and N. T. Porile, J. Inorg. Nucl. Chem. 30, 2027 (1968).
[4]E. Hagebo and H. Ravn, J. Inorg. Nucl. Chem. 31, 2649 (1969).
[5]J. A. Panontin and N. T. Porile, J. Inorg. Nucl. Chem. 32, 1775 (1970).
[6]K. Beg and N. T. Porile, Phys. Rev. C 3, 1631 (1971).
[7]J. B. Cumming and K. Bächmann, Phys. Rev. C 6, 1362 (1972).
[8]Y. W. Yu and N. T. Porile, Phys. Rev. C 7, 1597 (1973).

[9]Y. W. Yu, N. T. Porile, R. Warasila, and O. A. Schaeffer, Phys. Rev. C 8, 1091 (1973).
[10]P. M. Starzyk and N. Sugarman, Phys. Rev. C 8, 1448 (1973).
[11]S. Biswas and N. T. Porile, Phys. Rev. C 20, 1467 (1979).
[12]M. Lagarde-Simonoff and G. N. Simonoff, Phys. Rev. C 20, 1498 (1979).
[13]N. T. Porile, S. Pandian, H. Klonk, C. R. Rudy, and E. P. Steinberg, Phys. Rev. C 19, 1832 (1979).
[14]S. Pandian and N. T. Porile, Phys. Rev. C 23, 427 (1981).
[15]M. Lagarde-Simonoff, S. Regnier, H. Sauvageon, and G. N. Simonoff, Nucl. Phys. A260, 369 (1976).
[16]J. Tobailem, C. H. de Lassus St. Geniès, and L. Lévêque, Saclay Report No. CEA-N-1466 (1), 1971.
[17]S. Regnier, Ph.D. thesis, No. 557, Université de Bordeaux I, 1977.
[18]H. Sauvageon, Ph.D. thesis, No. 670, Université de Bordeaux I, 1981.
[19]N. Sugarman, M. Campos, and K. Wielgoz, Phys. Rev. 101, 388 (1956).
[20]N. T. Porile and N. Sugarman, Phys. Rev. 107, 1410 (1957).
[21]N. Sugarman, H. Münzel, J. A. Panontin, K. Wielgoz, M. V. Ramaniah, G. Lange, and E. Lopez-Menchero, Phys. Rev. 143, 952 (1966).
[22]L. C. Northcliffe and R. E. Schilling, Nucl. Data A7, 233 (1970).
[23]N. Metropolis, R. Bivins, M. Storm, A. Turkevich, J. M. Miller, and G. Friedlander, Phys. Rev. 110, 185 (1958).
[24]N. T. Porile, Phys. Rev. 120, 572 (1960).
[25]S. B. Kaufman, E. P. Steinberg, and M. W. Weisfield, Phys. Rev. C 18, 1349 (1978).
[26]S. Regnier, Phys. Rev. C 20, 1517 (1979).
[27]S. R. Nix and W. J. Swiatecki, Nucl. Phys. 71, 1 (1965).
[28]N. T. Porile and N. Sugarman, Phys. Rev. 107, 1422 (1957).
[29]W. Busza in *High Energy Physics and Nuclear Structure—1975 (Santa Fe and Los Alamos)*, Proceedings of the Sixth International Conference on High Energy Physics and Nuclear Structure, edited by D. E. Nagh and A. S. Goldhaber (AIP, New York, 1975).
[30]G. Berlad, A. Dar, and G. Eilam, Phys. Rev. D 13, 161 (1976).
[31]M. Ta Chung, Phys. Rev. D 15, 197 (1977).
[32]K. Gottfried, Phys. Rev. Lett. 32, 957 (1974).
[33]B. D. Wilkins, S. B. Kaufman, E. P. Steinberg, J. A. Urbon, and D. J. Henderson, Phys. Rev. Lett. 43, 1080 (1979).